International Journal of Engineering and Technology Innovation, vol. 15, no. 3, 2025, pp. 276-285

Effect of Silicon Dioxide-Reinforcement on the Mechanical Properties of AZ91 Alloy through Equal Channel Angular Pressing

Song-Jeng Huang, Chi-En Liu*, Sathiyalingam Kannaiyan, Yudhistira Adityawardhana*

Department of Mechanical Engineering, National Taiwan University of Science and Technology, Taipei, Taiwan, ROC

Received 05 January 2025; received in revised form 21 March 2025; accepted 24 March 2025

DOI: https://doi.org/10.46604/ijeti.2024.14712

Abstract

This study aims to investigate the enhancement of AZ91 magnesium-aluminum alloy by reinforcing it with 3 wt.% silicon dioxide and processing it through Equal Channel Angular Pressing (ECAP). Specimens with 0 wt.% and 3 wt.% silicon dioxide are fabricated using gravity casting and mechanical stirring, followed by T4 heat treatment and ECAP. Microstructural analysis using scanning electron microscopy (SEM) and X-ray diffraction (XRD) reveals that silicon dioxide is uniformly dispersed, refining the grain structure and dissolving the β-phase, leading to improved ductility. Mechanical testing shows that adding 3 wt.% silicon dioxide increases the yield strength (YS) by 15.26% and the ultimate tensile strength (UTS) by 23.65% after T4 treatment. ECAP further enhances these values by 19.92% and 41.35%, respectively, while increasing hardness by 15.95%. The improved strength-to-weight ratio makes this alloy suitable for automotive, aerospace, and electronics applications, particularly for lightweight structural components.

Keywords: AZ91, silicon dioxide, mechanical properties, heat treatment, ECAP

1. Introduction

Magnesium alloys have become a focal point in industrial applications owing to their lightweight, high specific strength, and excellent damping capacity. With a low density of approximately 1.73 g/cm^3, magnesium alloys are two-thirds lighter than aluminum and one-fourth the weight of iron, making them ideal for weight-sensitive designs. These materials are extensively used in the automotive, aerospace, and electronics industries to fabricate lightweight structures and improve energy efficiency [1-3]. In addition to their low density, magnesium alloys provide excellent damping performance, effectively absorbing impact loads, which makes them suitable for automotive components' vibration and noise control [4-5]. Their machinability is another advantage, enabling them to be processed into complex structures via methods such as extrusion, forging, and rolling. However, magnesium alloys face inherent challenges, such as limited strength and poor plasticity, which restrict their wider application [6-8].

To overcome these limitations, researchers have adopted various approaches, including heat treatments and severe plastic deformation (SPD) techniques. Among the SPD methods, Equal Channel Angular Pressing (ECAP) has demonstrated significant potential for refining microstructures, enhancing mechanical properties, and improving the overall performance of magnesium alloys [9-12]. Recent studies have highlighted several strategies for improving the mechanical properties of magnesium alloys. For example, Jamhari et al. [13] reviewed the effects of heat treatment parameters on the microstructure and

* Corresponding author. E-mail address: jien0921@gmail.com; yudhis1996@gmail.com

mechanical performance and demonstrated the role of optimized treatment in improving material properties. Similarly, Khayyamin et al. [14] investigated AZ91/SiO_2 composites fabricated by friction stir processing (FSP), revealing that grain refinement and uniform reinforcement particle distribution significantly enhanced the microhardness and tensile properties of the composites.

ECAP has been extensively studied as a method for improving magnesium alloys. Sahoo et al. [15] demonstrated that multi-pass ECAP effectively refined the grain size and enhanced the mechanical properties of RZ5 magnesium alloy sheets. Naseri et al. [16] reviewed the role of SPD in improving high-entropy alloys, emphasizing its transformative effects on grain structure and mechanical properties. The addition of reinforcements, such as silicon dioxide (SiO_2), has also been explored to enhance magnesium alloys. Zheng et al. [17] investigated the effects of homogenization treatments on AZ91. It was concluded that the dendritic β-phase ($Mg_{17}Al_{12}$) can be transformed into fine, uniformly distributed particles. This transformation leads to improved strength and ductility.

Despite the progress in magnesium alloy research, the combined application of SiO_2 reinforcement and ECAP remains underexplored. While previous studies have individually highlighted the benefits of micro-reinforcements and SPD techniques, the synergistic effects of combining SiO_2 reinforcement and ECAP on AZ91 magnesium alloy have not been fully investigated. To address this research gap, the present study examines how these two approaches interact to enhance the microstructure and mechanical properties of AZ91.

This study aims to investigate the combined effects of 3 wt.% SiO_2 reinforcement and ECAP on the AZ91 magnesium alloy. By utilizing advanced processing techniques, such as gravity casting, T4 heat treatment, and ECAP, this study aims to demonstrate the synergistic effects of SiO_2 reinforcement and SPD, providing insights into optimizing AZ91 magnesium alloy for industrial applications.

2. Methodology

This section presents the experimental procedures used to evaluate the influence of SiO_2 micro-reinforcement and ECAP on AZ91 magnesium alloy. The methodology includes material selection, sample preparation, heat treatment, and detailed characterization using X-ray diffraction (XRD), scanning electron microscopy (SEM), optical microscopy (OM), hardness, and tensile testing. The purpose is to correlate processing parameters with resulting microstructural and mechanical changes, ensuring consistency and reproducibility.

2.1. Material

SiO_2 powder was produced by Emperor Chemical Co., Ltd., Taipei, Taiwan, and had an average particle size of 63 μm. The selected particle size ensures suitable distribution within the AZ91 matrix and promotes effective load transfer between the reinforcement and the base alloy during mechanical testing. SiO_2 is chemically stable and offers high hardness, rendering it a suitable reinforcement material for enhancing the strength and wear resistance of magnesium alloys.

The base matrix material, AZ91 magnesium alloy, was procured from Jiehan Technology Co., Ltd., Taichung, Taiwan. AZ91 is a widely used commercial magnesium alloy that contains approximately 9% aluminum and 1% zinc, offering a good balance between castability, mechanical performance, and corrosion resistance. The detailed chemical composition of AZ91 is provided in Table 1. The materials were carefully selected to evaluate the synergistic effects of SiO_2 reinforcement and ECAP on microstructure and mechanical behavior.

Table 1 Chemical composition of AZ91

Elements	Al	Zn	Mn	Fe	Si	Cu	Ni	Mg
Wt.% concentration	8.95	0.84	0.26	0.005	0.009	0.008	0.0007	Balance

2.2. Material preparation

In this study, the AZ91 magnesium alloy was used as the base material, with SiO_2 chosen as the reinforcing element, which was added at ratios of 0 and 3 wt%. Ingots were prepared using gravity casting and mechanical stirring, as shown in Fig. 1. The ingots underwent T4 heat treatment, where the temperature was increased at a rate of 5 ℃/min to 260 ℃ and held for 1 hour to release residual stress. Subsequently, the ingots were slowly heated at a rate of 1 ℃/min over approximately 2 hours to 400 ℃, at which point they were held for 24 hours. After heat treatment, the ingots were cut into ECAP test bars. ECAP processing was conducted at 350 ℃ with a channel angle of 120°.

The melting was carried out in a resistance furnace, where the base material and reinforcing elements were first heated to 400 ℃ using sulfur hexafluoride (SF_6) gas. As the temperature increased to 600 ℃, argon gas was introduced to protect the molten metal. Upon reaching 750 ℃, the mixture was stirred for 20 minutes to disperse the reinforcing elements and then allowed to rest for 10 minutes. The plunger was lifted to allow the molten material to flow into the molds. Once naturally cooled, the material was removed, and the power source was turned off.

The removal of both extremities was due to the higher defect rates at the heads and tails of the ingots. The remaining material was then cut into ECAP test bars measuring 11.5 mm × 11.5 mm × 75 mm. The cut test bars underwent T4 solution treatment with a temperature increase of 5 ℃/min to 260 ℃, held for 1 hour to release residual stress, followed by a slow increase of 1 ℃/min over about 2 hours to 400 ℃, held for 24 hours, and then quenched in water. The surface oxidation layer of the test bars was removed by wet grinding with grits of #120, #240, #400, #600, #1000, #2000, and #4000.

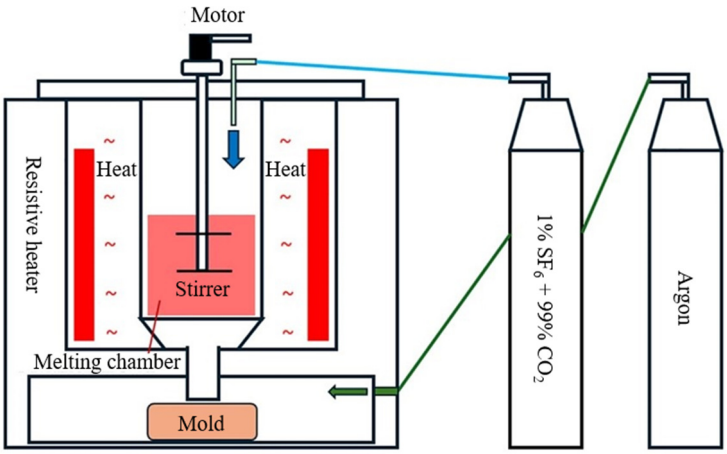

Fig. 1 Schematic of the furnace used for resistive gravity casting

2.3. Microstructural characterization

XRD analysis was conducted using a Bruker D2 PHASER X-ray diffractometer (Bruker Co., Boston, MA, USA) to investigate the crystalline structure within the 20° to 80° range at a scan rate of 0.04°/s. Data analysis was conducted using Bruker EVA 5.2 software (Bruker Co., Boston, MA, USA). This setup enabled a detailed examination of the material's crystalline phases and their respective structures. OM was performed using a Zeiss Axiotech 25 HD microscope (Oberkochen, Germany). The samples were meticulously prepared for observation by wet grinding with 4000-grit sandpaper and polishing with a slurry composed of 50-nm aluminum oxide powder and deionized water in a 1:5 ratio. This preparation ensured a smooth and uniform surface for detailed optical analysis. An appropriate etchant, as detailed in Table 2 (Emperor Chemical Co., Ltd., Taipei, Taiwan), was subsequently applied to reveal the metallographic structures. The microscope allowed for a detailed examination of the material's macroscopic morphology, grain size, and any present defects.

Table 2 Combinations of etching solutions

Ethanol (mL)	DI water (mL)	Acetic acid (mL)	Picric acid (mL)	Time (s)
7	1	1	1.2	3

2.4. Mechanical characterization

For hardness testing, a Vickers hardness tester (FR-1AN, Tokyo, Japan) was used to measure the hardness of the samples, ensuring precise and consistent results. The Vickers method employs a pyramidal diamond indenter under a specific load to create indentations on the sample surface, from which the hardness values are calculated. Each test was conducted on two samples, with five measurements taken from different locations: four at the corners and one at the center. The final hardness value was reported as the average of these measurements to ensure accuracy and minimize local variations. This testing provided crucial data on material resistance to deformation and wear.

For tensile testing, an MTS Insight 10 (MTS Systems Corp., Cary, NC, USA) tensile testing machine was used. This equipment was used to evaluate the mechanical properties of the samples, including the tensile strength, yield strength (YS), and elongation (EL). The machine provided precise control and accurate measurements of the applied forces and resulting deformations, enabling a comprehensive assessment of the material's tensile performance. Each test condition was evaluated using three samples to ensure statistical reliability. The tensile tests were conducted at a strain rate of 0.5 mm/min following the ASTM International Standard E8: Standard Test Methods for Tension Testing of Metallic Materials (ASTM E8) standard. The final values for YS, ultimate tensile strength (UTS), and EL were reported as the average of these three measurements.

3. Result and Discussion

This section presents the microstructural and mechanical characterization results of AZ91 and AZ91 + 3 wt.% SiO_2 under different processing conditions. The discussion is based on XRD, OM, SEM, energy-dispersive spectrometry (EDS), tensile, and hardness analyses. These findings provide insight into the relationship between material processing, phase transformation, grain refinement, and the resulting mechanical performance.

3.1. Material characterization

As shown in Fig. 2, the XRD analysis of AZ91 alloy and AZ91 + 3 wt.% SiO_2 alloy indicates that these alloys were composed of the α-phase $Mg_{0.97}Zn_{0.03}$ and the β-phase $Mg_{17}Al_{12}$. After T4 heat treatment, the intensities of the β-phase $Mg_{17}Al_{12}$ at $2\theta = 35°–45°$, specifically the (411) and (332) peaks, significantly decreased. This indicates the homogenization and dissolution of the β-phase $Mg_{17}Al_{12}$. Furthermore, after the ECAP treatment, only the peaks of the α-phase $Mg_{0.97}Zn_{0.03}$ were observed. Such a phenomenon is likely due to heating during the pre-ECAP and ECAP processes. These XRD results were consistent with the observations from OM.

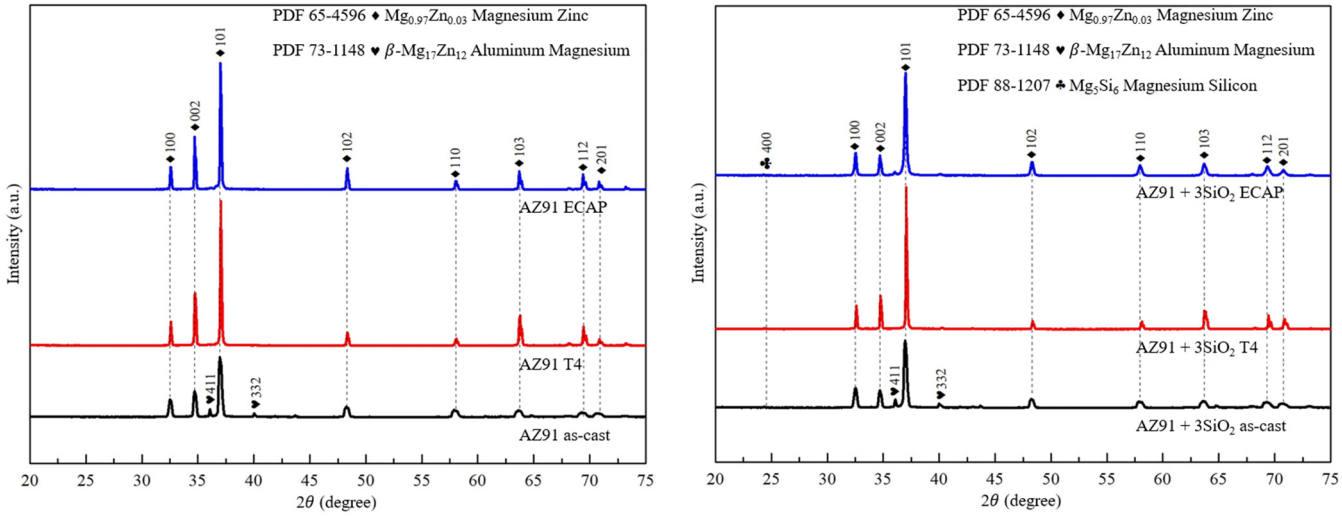

(a) Fabricated AZ91 (b) Fabricated AZ91 + 3 wt.% SiO_2

Fig. 2 XRD patterns of AZ91 and AZ91 + 3 wt.% SiO_2 under different processing conditions

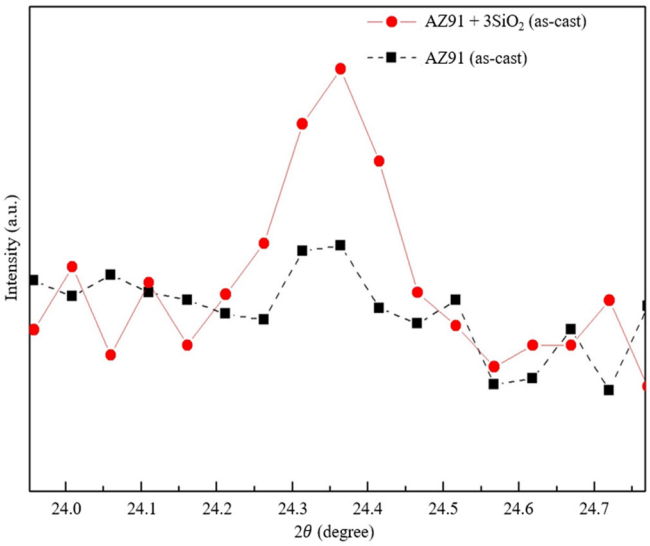

(c) Compared to the peak of as-cast

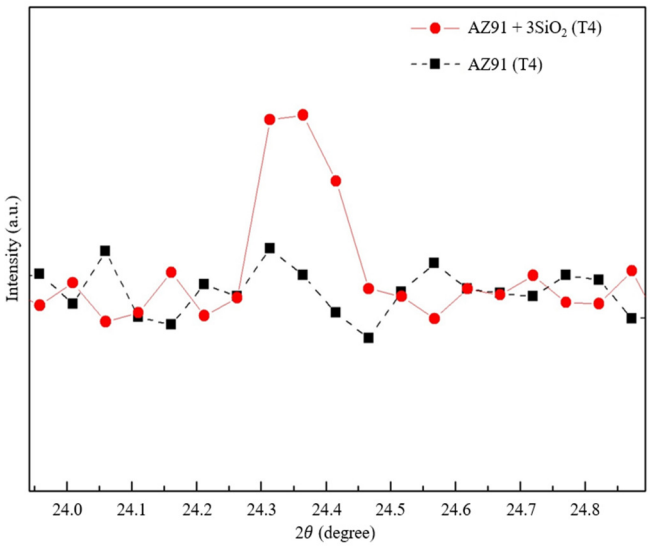

(d) Compared to the peak of T4

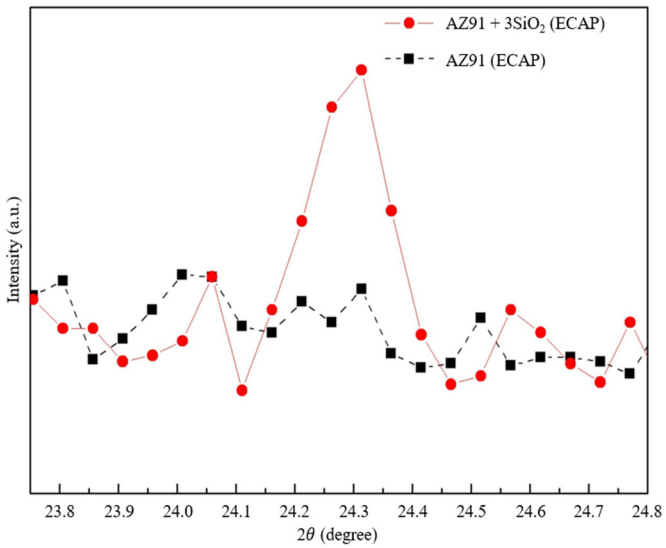

(e) Compared to the peak of ECAP

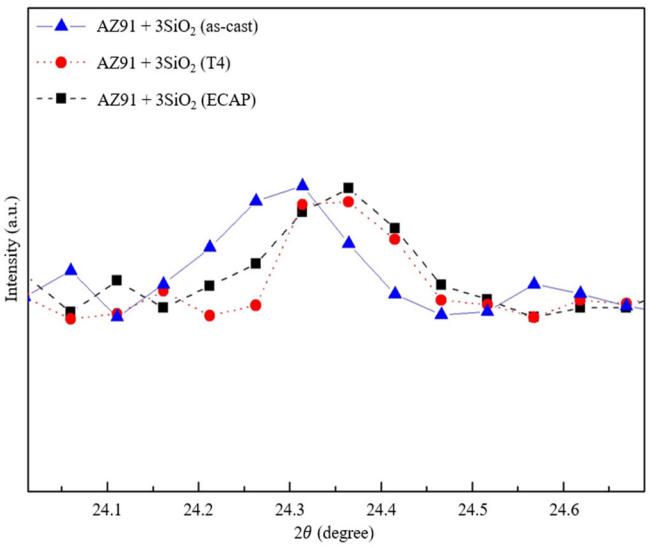

(f) Compared to the peak of a summary of all composites

Fig. 2 XRD patterns of AZ91 and AZ91 + 3 wt.% SiO_2 under different processing conditions (continued)

The reinforcing-phase SiO_2 added in this study exhibited peaks in the range of $2\theta = 24.1°–24.5°$. The XRD phase diagram indicates that the SiO_2 dissolved to form Mg_5Si_6, which can be observed through EDS and SEM images. Consistent with previous studies, the peak intensity of the β-phase $Mg_{17}Al_{12}$ in the magnesium alloy decreased upon solution heat treatment. This phenomenon, which is also observed in the OM images, suggests that the β-phase dissolves into the matrix, thereby increasing the ductility of the material while decreasing its strength and hardness. These findings are consistent with the tensile test results of this study.

Fig. 3 below displays the results of the OM analysis, including images of the as-cast, homogenized, and ECAP states. Figs. 3(d)-(f) depict the AZ91 alloy with the added reinforcing phase, whereas Figs. 3(a)-(c) show AZ91 without the reinforcing phase. A noticeable grain refinement can be observed. As observed in Figs. 3(a) and (d), the formation of numerous secondary β-phase $Mg_{17}Al_{12}$, marked by arrows at the grain boundaries, is evident and consistent with previous research findings. After solution heat treatment, as shown in Figs. 3(b) and (e), the β-phase $Mg_{17}Al_{12}$ dissolves into the α-phase $Mg_{0.97}Zn_{0.03}$, resulting in its substantial disappearance in the OM images. This observation is consistent with the XRD analysis, which revealed a reduction in the β-phase $Mg_{17}Al_{12}$ peaks. Figs. 3(c) and (f) show the OM images after ECAP, in which grain refinement is observed within the circles. This result is attributed to dynamic recrystallization (DRX) induced by the severe plastic deformation ECAP.

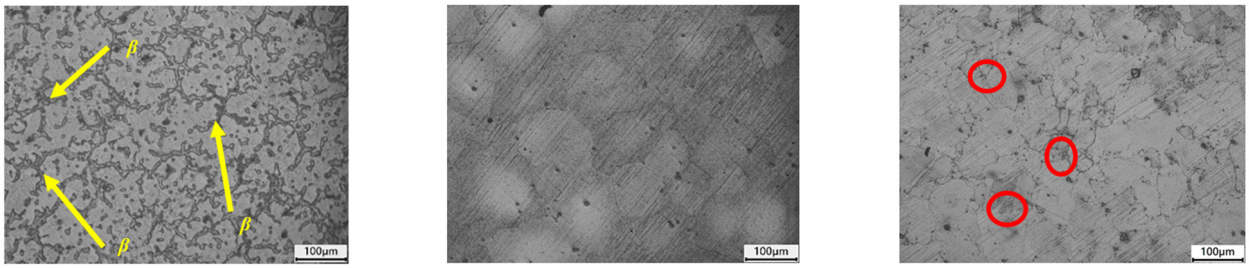

(a) AZ91 (as-cast) (b) AZ91 (T4) (c) AZ91 (ECAP)

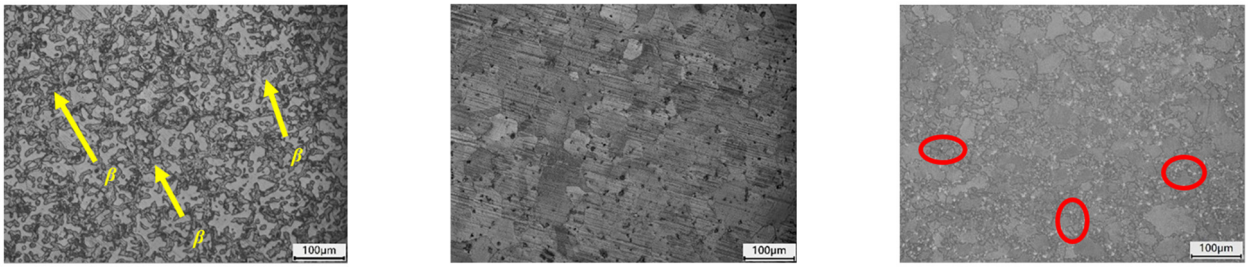

(d) AZ91 + 3 wt.% SiO_2 (as-cast) (e) AZ91 + 3 wt.% SiO_2 (T4) (f) AZ91 + 3 wt.% SiO_2 (ECAP)

Fig. 3 Optical microscopy images of AZ91 and AZ91 + 3 wt.% SiO_2 under different processing conditions

The grain size analysis revealed the OM size distribution of the alloys after the T4 heat treatment. The average grain sizes were 78.02 ± 11.21 μm for AZ91 and 46.93 ± 10.22 μm for AZ91 + 3 wt.% SiO_2. After ECAP treatment, the OM size distribution of the alloys was 34.26 ± 13.68 μm for AZ91 and 22.04 ± 1.45 μm for AZ91 + 3 wt.% SiO_2. The OM images demonstrate that SPD significantly improved the microstructure, thereby promoting grain refinement. The results indicate that the addition of the reinforcing phase SiO_2 led to a more pronounced grain refinement effect, which subsequently enhanced the mechanical properties of the alloy. Fig. 4 displays the SEM and EDS results for AZ91 and AZ91 + 3 wt.% SiO_2. The images show that the secondary phase in AZ91 is primarily composed of Mg-Al, forming irregular shapes with uneven distribution. In contrast, AZ91 + 3 wt.% SiO_2 exhibited both a secondary phase and the Mg-Si phase. These observations are consistent with the peaks detected by XRD analysis. The distribution and structure of these phases affect the alloy's strength.

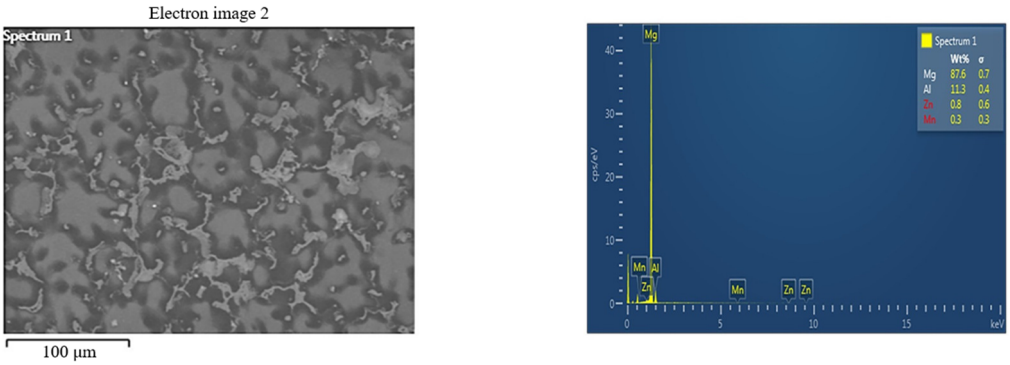

(a) SEM image of AZ91 (as-cast) (b) EDS spectrum of AZ91 (as-cast)

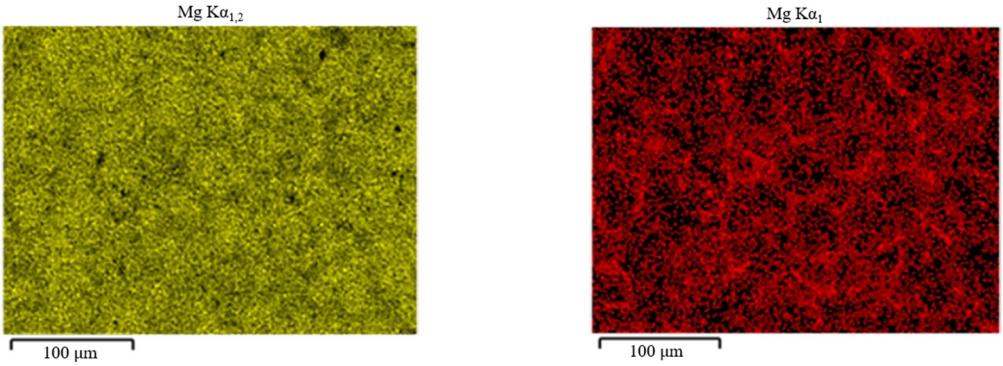

(c) Mg mapping of AZ91 (as-cast) (d) Al mapping of AZ91 (as-cast)

Fig. 4 SEM images and EDS elemental maps of AZ91 and AZ91 + 3 wt.% SiO_2 in the as-cast condition

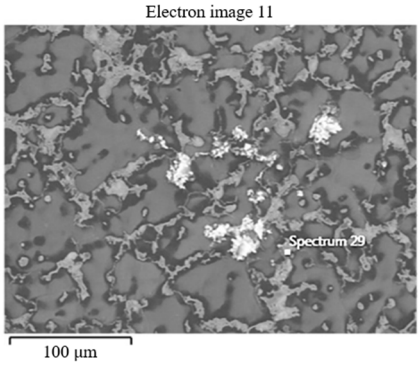

(e) SEM image of AZ91 + 3 wt.% SiO_2 (as-cast)

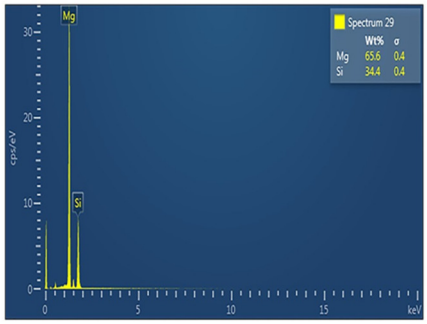

(f) EDS spectrum of + 3 wt.% SiO_2 (as-cast)

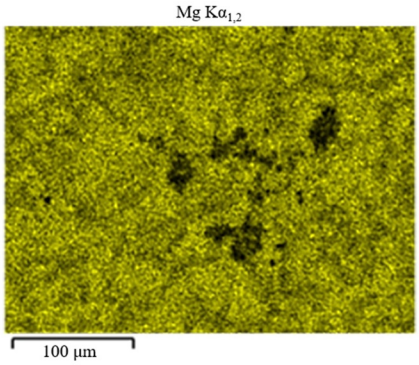

(g) Mg mapping of AZ91 + 3 wt.% SiO_2 (as-cast)

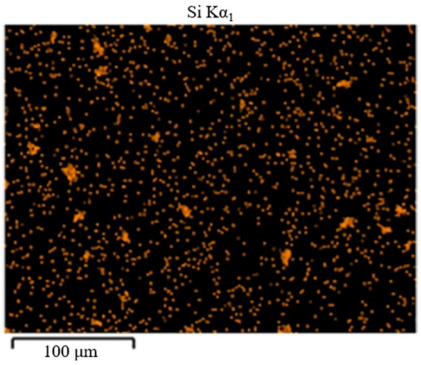

(h) Si mapping of AZ91 + 3 wt.% SiO_2 (as-cast)

Fig. 4 SEM images and EDS elemental maps of AZ91 and AZ91 + 3 wt.% SiO_2 in the as-cast condition (continued)

3.2. Tensile and hardness tests

The stress-strain curves for AZ91 and AZ91 + 3 wt.% SiO_2 under as-cast, T4, and ECAP conditions are shown in Fig. 5. As indicated in Table 3, the material exhibited improved ductility after T4 and ECAP. After the T4 homogenization heat treatment, the ductility of AZ91 increased, with the YS and UTS reaching 106.77 MPa and 215 MPa, respectively, representing increases of 0.84% and 22.77%. The elongation (EL) improved from 4.03% to 12.67%. Following ECAP treatment, AZ91 showed an upward trend in YS and UTS, with values of 129.99 MPa and 268.13 MPa, respectively, representing increases of 22.77% and 46.39%. The EL further improved to 19.17%.

Table 3 shows the mechanical properties of all composites. For AZ91 + 3 wt.% SiO_2, the T4 homogenization heat treatment increased the YS to 126.36 MPa and the UTS to 260.87 MPa, representing increases of 15.26% and 23.65%, respectively. The EL improved from 4.03% to 17.87%. After ECAP treatment, AZ91 + 3 wt.% SiO_2 exhibited the highest mechanical properties, with the YS and UTS reaching 131.47 MPa and 298.2 MPa, representing increases of 19.92% and 41.35%, respectively. The EL improved to 28.97%.

The effects of T4 heat treatment can be inferred from the XRD analysis, which reveals a decrease in the β-phase $Mg_{17}Al_{12}$ peaks, and from the OM analysis, indicating that the β-phase has largely dissolved into the matrix. The β-phase $Mg_{17}Al_{12}$ affects the mechanical properties by acting as a strengthening phase in as-cast AZ91 alloys but reduces ductility due to its brittle nature. After the T4 heat treatment, the alloy dissolves into the α-phase matrix, improving the ductility and homogenizing the alloy. The ECAP results are consistent with those of previous studies, showing that the material's ductility improved due to DRX and the T4 and heating processes conducted during ECAP [18].

In the as-cast AZ91 alloy, the presence of an eutectic network, primarily composed of the β-phase ($Mg_{17}Al_{12}$), results in the deterioration of mechanical properties by acting as a brittle phase and stress concentrator. Plastic deformation methods such as ECAP can effectively break down this eutectic network, leading to a more homogeneous microstructure and improved

mechanical properties [19-20]. Specifically, DRX during ECAP refines the microstructure, reducing the continuity of the eutectic network and enhancing ductility and strength. Hardness testing indicated a slight decrease in the hardness of both materials after T4 heat treatment, with the hardness of AZ91 + 3 wt.% SiO_2 decreasing by 10.01%.

This decrease suggests that the T4 heat treatment resulted in significant dissolution of the β-phase into the α-phase in AZ91 + 3 wt.% SiO_2, reducing the material's hardness but improving its ductility. This suggests that the T4 heat treatment caused significant incorporation of the β-phase into the α-phase in AZ91 + 3 wt.% SiO_2. After ECAP treatment, the grain size of AZ91 was significantly refined, and its hardness was increased to 96.3 HV. This increase in hardness after ECAP treatment is attributed to the grain refinement and the effect of work hardening, further supported by the breakdown of the eutectic network, which reduces stress concentration points. The hardness of AZ91 + 3 wt.% SiO_2 also increased after ECAP, consistent with the enhanced mechanical properties observed in the tensile tests.

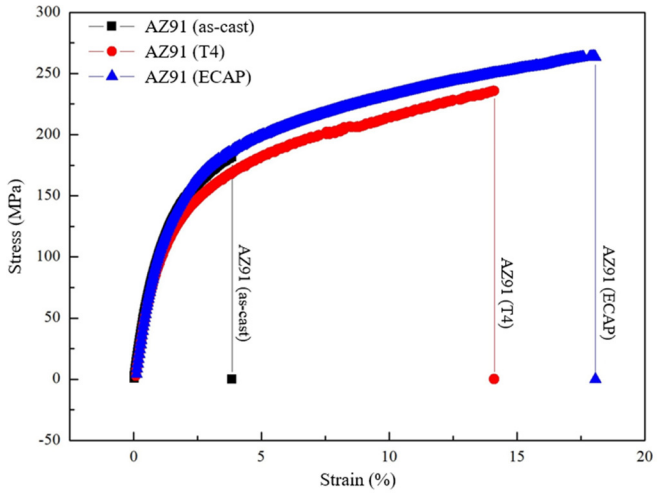

(a) Stress-strain curve of AZ91

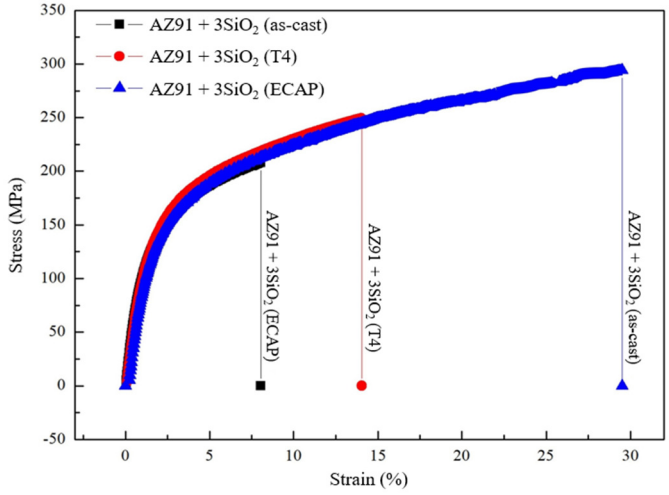

(b) Stress-strain curve of AZ91 + 3 wt.% SiO_2

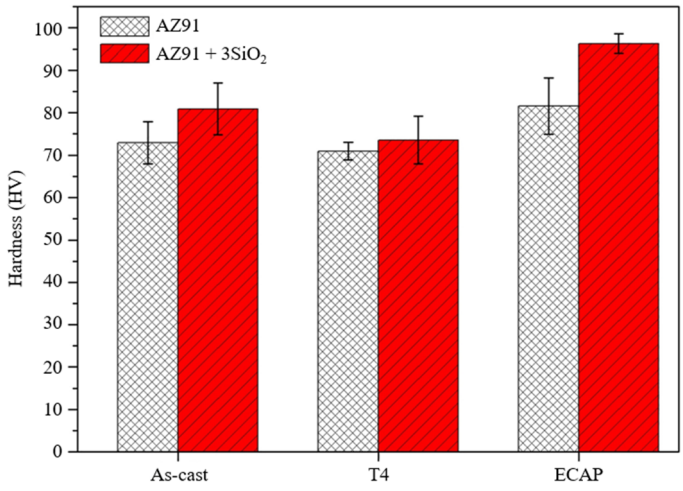

(c) Vickers hardness

Fig. 5 Stress-strain curves and vickers hardness of AZ91 and AZ91 + 3 wt.% SiO_2

Table 3 Mechanical characteristics of AZ91 and AZ91+ 3 wt.% SiO_2

Sample	Process	YS (MPa)	UTS (MPa)	EL (%)	Hardness (HV)
AZ91	as-cast	105.88	183.17	4.03	72.89 ± 5.00
	T4	106.77	215.00	12.67	70.95 ± 2.11
	ECAP	129.99	268.13	19.17	81.55 ± 6.63
AZ91 + 3 wt.% SiO_2	as-cast	109.63	210.97	8.59	80.92 ± 6.09
	T4	126.36	260.87	17.87	73.56 ± 5.58
	ECAP	131.47	298.20	28.97	96.28 ± 2.29

4. Conclusion

In this study, AZ91 magnesium-aluminum alloy was selected as the matrix material and reinforced with 3 wt.% SiO_2 to investigate the effects of micro-reinforcement and ECAP on its structural and mechanical properties. The experimental process involved gravity casting, mechanical stirring, T4 heat treatment, and ECAP. The results demonstrated significant grain refinement and notable improvements in strength, ductility, and hardness.

(1) Microstructural refinement: SiO_2 particles were uniformly dispersed within the AZ91 matrix, leading to significant grain refinement, while the T4 heat treatment dissolved the β-phase ($Mg_{17}Al_{12}$) into the α-phase to improve ductility and microstructural homogeneity, and DRX during ECAP further enhanced the grain structure and mechanical properties.

(2) Mechanical enhancements: The addition of 3 wt.% SiO_2 resulted in a 15.26% increase in YS and a 23.65% improvement in UTS after T4 treatment, while ECAP processing further enhanced the YS by 19.92%, the UTS by 41.35%, and Vickers hardness by 15.95%.

(3) Application potential: The SiO_2-reinforced AZ91 magnesium alloy demonstrates strong potential in weight-sensitive applications. Its enhanced mechanical properties and reduced density render it suitable for the automotive, aerospace, and electronics industries, where lightweight structures can improve fuel efficiency and performance.

The integration of SiO_2 reinforcement and ECAP processing provides a cost-effective approach to optimizing magnesium alloys for engine components, fuselage structures, and electronic casings. These findings lay the foundation for further research and industrial applications of ECAP-processed magnesium alloys in advanced engineering fields.

Acknowledgments

The authors extend their appreciation to the National Science and Technology Council, Taiwan, for their financial support in the form of project grant number NSTC 111-2221-E-011-096-MY3.

Conflicts of Interest

The authors declare no conflict of interest.

References

[1] R. V. Marode, T. A. Lemma, N. Sallih, S. R. Pedapati, M. Awang, and A. Hassan, "Research Progress in Friction Stir Processing of Magnesium Alloys and Their Metal Matrix Surface Composites: Evolution in the 21st Century," Journal of Magnesium and Alloys, vol. 12, no. 6, pp. 2091-2146, 2024.

[2] S. J. Huang, C. Li, M. Sarkar, W. Li, S. Kannaiyan, H. K. Bilgili, et al., "Mechanical Study Reinforced Magnesium-Yttrium Alloys by Eggshell Powder Using Resistance Casting," Journal of Alloys and Compounds, vol. 1008, article no. 176458, 2024.

[3] H. Geng, J. Shen, S. Hu, F. Zhang, and K. Geng, "Improving the Mechanical and Wear Properties of AZ91 Magnesium Alloy via Laser Cladded (AlCu)3.5CoCrNiSnx (x = 0 and 1) High Entropy Alloy Coatings," Results in Engineering, vol. 23, article no. 102778, 2024.

[4] S. J. Huang, J. Sanjaya, Y. Adityawardhana, and S. Kannaiyan, "Enhancing the Mechanical Properties of AM60B Magnesium Alloys through Graphene Addition: Characterization and Regression Analysis," Materials, vol. 17, no. 18, article no. 4673, 2024.

[5] S. S. Prasad, S. B. Prasad, K. Verma, R. K. Mishra, V. Kumar, and S. Singh, "The Role and Significance of Magnesium in Modern Day Research-A Review," Journal of Magnesium and Alloys, vol. 10, no. 1, pp. 1-61, 2022.

[6] M. K. Kulekci, "Magnesium and Its Alloys Applications in Automotive Industry," The International Journal of Advanced Manufacturing Technology, vol. 39, no. 9-10, pp. 851-865, 2008.

[7] S. Annamalai, S. Periyakgoundar, and S. Gunasekaran, "Magnesium Alloys: A Review of Applications," Materials and Technology, vol. 53, no. 6, pp. 881-890, 2019.

[8] Z. Zhang, K. Nie, K. Deng, and Y. J. Li, "Design and Preparation of High-Performance Dissolvable in-situ (MgO-Al3Fe)/AZ91 Magnesium Matrix Composites by Controlling the Content of Precursor Particles Combined with Low-Temperature Extrusion," Journal of Alloys and Compounds, vol. 1020, article no. 179508, 2025.

[9] J. Song, J. She, D. Chen, and F. Pan, "Latest Research Advances on Magnesium and Magnesium Alloys Worldwide," Journal of Magnesium and Alloys, vol. 8, no. 1, pp. 1-41, 2020.

[10] S. J. Huanga, S. Kannaiyan, and M. Subramani, "Effect of Nano-Nb2O5 on the Microstructure and Mechanical Properties of AZ31 Alloy Matrix Nanocomposites," Advances in Nano Research, vol. 13, no. 4, pp. 407-416, 2022.

[11] S. J. Huang, M. P. Mose, and S. Kannaiyan, "A Study of the Mechanical Properties of AZ61 Magnesium Composite After Equal Channel Angular Processing in Conjunction with Machine Learning," Materials Today Communication, vol. 33, article no. 104707, 2022.

[12] S. Kandemir, J. Bohlen, and H. Dieringa, "Influence of Recycled Carbon Fiber Addition on the Microstructure and Creep Response of Extruded AZ91 Magnesium Alloy," Journal of Magnesium and Alloys, vol. 11, no. 7, pp. 2518-2529, 2023.

[13] F. I. Jamhari, F. M. Foudzi, M. A. Buhairi, A. B. Sulong, N. A. M. Radzuan, N. Muhamad, et al., "Influence of Heat Treatment Parameters on Microstructure and Mechanical Performance of Titanium Alloy in LPBF: A Brief Review," Journal of Materials Research and Technology, vol. 24, pp. 4091-4110, 2023.

[14] D. Khayyamin, A. Mostafapour, and R. Keshmiri, "The Effect of Process Parameters on Microstructural Characteristics of AZ91/SiO2 Composite Fabricated by FSP," Materials Science and Engineering: A, vol. 559, pp. 217-221, 2013.

[15] P. S. Sahoo, M. M. Mahapatra, P. R. Vundavilli, R. K. Sabat, S. Sirohi, and S. Kumar, "Investigation of Severe Plastic Deformation Effects on Magnesium RZ5 Alloy Sheets Using a Modified Multi-Pass Equal Channel Angular Pressing (ECAP) Technique," Materials, vol. 16, no. 14, article no. 5158, 2023.

[16] M. Naseri, A. O. Moghadam, M. Anandkumar, S. Sudarsan, E. Bodrov, M. Samodurova, et al., "Enhancing the Mechanical Properties of High-Entropy Alloys Through Severe Plastic Deformation: A Review," Journal of Alloys and Metallurgical Systems, vol. 5, article no. 100054, 2024.

[17] L. Zheng, H. Nie, W. Liang, H. Wang, and Y. Wang, "Effect of Pre-Homogenizing Treatment on Microstructure and Mechanical Properties of Hot-Rolled AZ91 Magnesium Alloys," Journal of Magnesium and Alloys, vol. 4, no. 2, pp. 115-122, 2016.

[18] S. J. Huang, Y. Adityawardhana, and S. Kannaiyan, "Enhancement Strength of AZ91 Magnesium Alloy Composites Reinforced with Graphene by T6 Heat Treatment and Equal Channel Angular Pressing," Archives of Civil and Mechanical Engineering, vol. 24, no. 4, article no. 235, 2024.

[19] Z. Nasiri, M. S. Khorrami, H. Mirzadeh, and M. Emamy, "Enhanced Mechanical Properties of As-Cast Mg-Al-Ca Magnesium Alloys by Friction Stir Processing," Materials Letters, vol. 296, article no. 129880, 2021.

[20] M. S. Mehranpour, A. Heydarinia, M. Emamy, H. Mirzadeh, A. Koushki, and R. Razi, "Enhanced Mechanical Properties of AZ91 Magnesium Alloy by Inoculation and Hot Deformation," Materials Science and Engineering: A, vol. 802, article no. 140667, 2021.